

# Nucleation and Growth of the HfO<sub>2</sub> Dielectric Layer for Graphene-Based Devices

Il-Kwon Oh,<sup>†</sup> Jukka Tanskanen,<sup>‡</sup> Hanearl Jung,<sup>†</sup> Kangsik Kim,<sup>#</sup> Mi Jin Lee,<sup>#</sup> Zonghoon Lee,<sup>#</sup> Seoung-Ki Lee,<sup>†</sup> Jong-Hyun Ahn,<sup>†</sup> Chang Wan Lee,<sup>†</sup> Kwanpyo Kim,<sup>||</sup> Hyungjun Kim,<sup>\*,†</sup> and Han-Bo-Ram Lee<sup>\*,†,⊥</sup>

<sup>†</sup>School of Electrical and Electronic Engineering, Yonsei University, Seoul 120-749, Korea

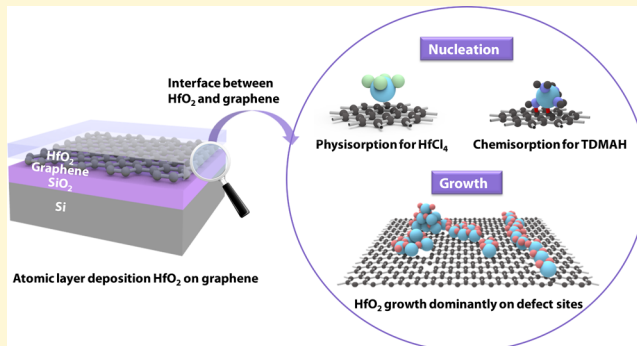
<sup>‡</sup>Department of Chemistry, University of Eastern Finland, Joensuu 80101, Finland

<sup>#</sup>School of Materials Science and Engineering and <sup>||</sup>Department of Physics, Ulsan National Institute of Science and Technology (UNIST), Ulsan 689-798, Korea

<sup>⊥</sup>Department of Materials Science and Engineering, Incheon National University, 406-840 Incheon, Korea

## Supporting Information

**ABSTRACT:** We investigated nucleation and growth characteristics of atomic layer deposition (ALD) HfO<sub>2</sub> on exfoliated and chemical vapor deposition (CVD) graphene by using two Hf precursors, tetrakis(dimethylamino)hafnium (TDMAH) and hafnium tetrachloride (HfCl<sub>4</sub>). Experimental results and theoretical calculations indicate that HfO<sub>2</sub> nucleation is more favorable on CVD graphene than on exfoliated graphene due to the existence of defect sites. Also, the TDMAH precursor showed much more unfavorable nucleation and growth than HfCl<sub>4</sub> due to different initial adsorption mechanisms, affecting lower leakage currents and breakdown electric field. ALD growth characteristics of HfO<sub>2</sub> will be fundamentally and practically significant for realizing the fabrication of graphene-based electronic devices.



## INTRODUCTION

Graphene has attracted a great deal of attention for potential applications in electronic devices due to its novel electrical properties, such as high electron and hole mobility above 100,000 cm<sup>2</sup>/(V s).<sup>1</sup> In order to realize graphene-based electronic devices, high quality high-k dielectric thin films are required.<sup>2</sup> However, since conventional techniques of thin film deposition employ energetic radicals in the plasma state for sputtering or chemical reactions of precursors for chemical vapor deposition (CVD), the physical properties of graphene which is composed of an ideal single atomic layer are easily affected by deposition environments.<sup>3</sup> Thus, the damage-free deposition method is needed to form high-k dielectrics on graphene. Compared to other deposition techniques, atomic layer deposition (ALD) produces dense and pinhole-free since ALD films are formed through a layer-by-layer growth manner based on the surface self-saturated reaction of precursors. In addition, damages on an original surface in ALD are less significant than those in CVD and physical vapor deposition (PVD).<sup>4</sup> Therefore, ALD has been one of the essential fabrication methods for graphene-based devices and has been widely used.

In earlier studies, ALD dielectrics such as Al<sub>2</sub>O<sub>3</sub> and HfO<sub>2</sub> were attempted on graphite surfaces which have chemically

identical surface properties to those of graphene.<sup>5–10</sup> Selective growth of ALD dielectrics along the step edge sites of highly ordered pyrolytic graphite (HOPG) was observed since the step edge sites are chemically more reactive than the basal planes.<sup>5–7</sup> In the following studies, dielectric deposition by ALD on graphene prepared from the exfoliation of HOPG shows similar results to previous reports about ALD on HOPG since there was no chemically available adsorption site on graphene surfaces.<sup>8–10</sup> In other research, interestingly, on graphene synthesized by CVD, there was no selectivity in the growth of ALD dielectrics rather island growth over all the surface.<sup>11–13</sup> Different growth behaviors of ALD dielectrics on graphene surfaces are probably affected by nonideal surface properties of graphene originating from different synthesis methods and preparation processes. Although exfoliated graphene from HOPG and CVD-grown graphene have been widely used to prepare graphene, however, there has been no systematic and comprehensive study on surface reactions between ALD precursors and graphene synthesized by various ways.

Received: April 1, 2015

Revised: August 10, 2015

Published: August 19, 2015

In addition, since it is hard to form a continuous high  $k$  dielectric layer on graphene which is essential to fabricate electronic devices using graphene, researchers have tried several surface treatments on graphene to improve nucleation of ALD high  $k$  layer: the deposition and oxidation of metal films,<sup>14–19</sup> functionalization of graphene via ozone,<sup>20,21</sup> O<sub>2</sub> plasma,<sup>22</sup> and nitrogen dioxide,<sup>23</sup> and the spin-coating of polymer films<sup>24,25</sup> and self-assembled monolayers<sup>26</sup> as seeding layers. However, the fundamental explanation and understanding of the surface reaction between precursors and graphene during ALD have remained unclear although the surface reaction is a key mechanism of ALD.

In this article, we mainly focused on the nucleation and growth mechanism of ALD HfO<sub>2</sub> on exfoliated graphene from HOPG and synthesized graphene by CVD. Based on the results, we extended our investigation to the effects of precursor on growth and nucleation by using two Hf precursors, tetrakis(dimethylamino)hafnium (TDMAH) and hafnium tetrachloride (HfCl<sub>4</sub>). Surface morphologies of ALD HfO<sub>2</sub> on graphene were characterized with increasing cycles. Nucleation and growth mechanism were studied by the correlation with analysis results including vibrational energy states, atomic scale image, crystallinity, and surface chemistry. In addition, activation energy and energetic of reaction pathways during the ALD process were investigated by quantum chemical calculations. The experimental results are discussed with the theoretical calculation results. Graphene-based devices using ALD HfO<sub>2</sub> dielectric were fabricated, and device performances were investigated by correlating the growth behaviors of ALD HfO<sub>2</sub>. This comparative research with experimental and theoretical results should have significant impacts on the fabrication of graphene-based electronic devices.

## ■ EXPERIMENTAL SECTION

**Graphene Preparation.** Graphene is prepared in two ways: one is mechanical exfoliation from HOPG and the other one is the CVD method. A piece of Scotch Tape was placed on HOPG and peeled away. The tape with graphite flakes detached from HOPG was folded and unfolded several times to reduce the adhesive force between the tape and flakes. The tape with flakes was placed on 300 nm SiO<sub>2</sub>/Si substrate, and the surface of the tape was gently rubbed with tweezers for a few minutes to transfer graphene layers from the tape to the substrate.<sup>27</sup> The transferred graphene layers on the SiO<sub>2</sub> substrate were confirmed by contrast difference in optical microscope images. Single layer graphene was synthesized by low pressure CVD which has been many times reported elsewhere.<sup>28</sup> A 25- $\mu$ m-thick Cu foil as a metal catalyst was placed at the center of a quartz tube of the CVD system and heated up to 1035 °C with a 25 °C/min ramping rate, under hydrogen ambient (flow rate of H<sub>2</sub> = 10 sccm). The Cu foil was annealed at 1035 °C in the same hydrogen flow for 2 h to eliminate a native copper oxide. After annealing, the Cu foil was exposed to CH<sub>4</sub> gas with the flow rate of 0.4 sccm for 4 h 30 min and cooled down to room temperature in the CVD chamber without any disturbance. Poly(methyl methacrylate) (PMMA) was spin-coated on the as-grown single layer graphene on the Cu foil, and the copper foil was etched out by using 0.1 M of ammonium persulfate etchant. The sample was rinsed in deionized water several times to remove residual etchant, and the PMMA/graphene layer was transferred to the SiO<sub>2</sub> substrate.<sup>29</sup> The PMMA supporting layer was removed by immersing the sample in acetone for ~12 h. For transmission electron microscopy (TEM) analysis before and after ALD on graphene, the graphene was transferred onto Quanti-foil TEM grids using a direct transfer method.<sup>30</sup> To bond graphene and the amorphous carbon (a-C) film of the TEM grid, the TEM grid is placed on the top of graphene on Cu, and isopropyl alcohol (IPA) is gently dropped on the top of the grid to wet both the a-C and graphene films. After surface tension

generates the contact between graphene and a-C by IPA evaporation, the sample was floated on the FeCl<sub>3</sub> aqueous solution (0.1 g/mL) to etch the Cu foil. After the transfer method, the grids were transferred to the ALD chamber, and then they were picked by Cu tongs to hold their positions during the ALD process. Graphene samples were loaded in the ALD chamber (NCD Co., Lucida M100-PL) and annealed at 450 °C with H<sub>2</sub> and Ar (flow rate of H<sub>2</sub> = 10 sccm and Ar = 10 sccm) to remove residual PMMA prior to ALD HfO<sub>2</sub>.

**ALD Process.** TDMAH and HfCl<sub>4</sub> precursors contained in a stainless-steel bubbler were evaporated at 40 and 170 °C, respectively, to obtain sufficient vapor pressure. Manifold lines were heated to 10–15 °C higher than the temperature of the bubbler to prevent precursor condensation. Evaporated precursor vapors were carried into the ALD chamber with Ar carrier gas of which the flow rate was controlled by a mass flow controller (MFC). Ar gas with the same flow rate was also used for the ALD purge step between each precursor and reactant exposure step. H<sub>2</sub>O was used for a counter reactant for both HfCl<sub>4</sub> and TDMAH. The substrate temperature was kept at 250 °C. On exfoliated and CVD graphene substrates, HfO<sub>2</sub> were deposited for various ALD cycles.

**Characterization of HfO<sub>2</sub> on Graphene.** Morphologies of ALD HfO<sub>2</sub> on graphene with increasing ALD cycles were characterized using atomic force microscopy (AFM; VEECO Co., Multimode model), field emission scanning electron microscopy (FE-SEM; JEOL Ltd., JSM-7001F model), and high resolution-TEM (HR-TEM; FEI Titan Cube G2 60-300) equipped with an image-aberration corrector and monochromator. The HR-TEM was operated at an accelerating voltage of 80 kV. In addition, HR-TEM images and the corresponding Fast Fourier Transform (FFT) patterns of the HfO<sub>2</sub> on graphene were obtained. The number of graphene layers, the presence of sp<sup>2</sup>–sp<sup>3</sup> hybridization, and defects were analyzed by using Raman spectroscopy (WITEC CRM200) with a 600 grooves/mm grating. The laser wavelength and power were 532 nm (Elaser = 2.33 eV) and 1.0 mW, respectively. Since the lateral analysis size of Raman spectroscopy is about 2  $\mu$ m  $\times$  2  $\mu$ m, graphene layers of which the lateral size was larger than 5  $\mu$ m  $\times$  5  $\mu$ m were picked from optical microscope analysis (Olympus bx41 with  $\times$ 100 LWD Plan objective lens, working distance = 2 mm). The chemical composition and bonding structure were analyzed by X-ray photoelectron spectroscopy (XPS; Thermo Scientific Co., K-Alpha model) with 1486.6 eV Al K $\alpha$  monochromatic source. HOPG was used instead of exfoliated graphene because the beam size of X-ray in the XPS system is bigger than the size of exfoliated graphene of which pieces are sparsely dispersed on the SiO<sub>2</sub> substrate.

**Quantum Chemical Calculation.** Full structural optimization computations at the density functional level of theory (DFT) were performed by the PBE0<sup>30,31</sup> functional with the standard split-valence + polarization (def-SVP)<sup>32,33</sup> basis set and without symmetry constraints. Quasirelativistic effective core potentials (ECP) were utilized for 60 core electrons of Hf.<sup>21</sup> The graphene basal plane was simulated by a C<sub>24</sub>H<sub>16</sub> cluster with H-terminated edges.<sup>34</sup> These clusters have been previously utilized in the investigation of Pt ALD on graphene.<sup>35</sup> A C<sub>50</sub>H<sub>16</sub> cluster with H-terminated edges and a diameter of about 1.5 nm was utilized to represent the local atomic structure of graphene grain boundary with pentagon–heptagon pairs. The MP2 calculations within the Resolution-of-the-Identity (RI)<sup>36,37</sup> approximation were performed by the TURBOMOLE<sup>38</sup> program package and by using a def2-TZVP<sup>34,39</sup> basis set as implemented in TURBOMOLE. Full structural RI-MP2 optimizations were performed on the DFT-optimized systems. The RI method means expansions of products of virtual and occupied orbitals by expansions of auxiliary functions, simplifying the computation and resulting in more efficient calculations as compared to standard MP2. The adsorption process of molecules on a surface can be divided into several subreactions, which is usually called a reaction pathway, for instance initial physisorption, transition site, product physisorbed, and final product. Energy barriers of each reaction step are calculated to find the total energy difference between initial chemical species and final products. In the reaction pathway calculations, verification of the transition states having only one imaginary vibrational mode and the stationary points being true

local minima took place by performing frequency calculations on the optimized structures. Both DFT and RI-MP2 energetics are given as reference to isolated gas phase reactants of  $\text{HfCl}_4$ , TDMAHf, and  $\text{H}_2\text{O}$  and the graphene clusters.

**Electrical Characterization.** Metal–insulator–graphene (MIG) capacitors were fabricated to evaluate dielectric and insulating properties of ALD  $\text{HfO}_2$  on graphene. CVD graphene transferred on 300 nm  $\text{SiO}_2/\text{Si}$  was used as a bottom layer of a capacitor. ALD  $\text{HfO}_2$  films using  $\text{HfCl}_4$  and TDMAH were deposited for 1000 cycles on the CVD graphene/ $\text{SiO}_2/\text{Si}$  substrate. The thickness of 1000 cycles of  $\text{HfO}_2$  measured by SEM is 98 nm for  $\text{HfCl}_4$  and 74 nm for TDMAH. Then, Al top electrode was defined with the size of  $3.14 \times 10^4 \mu\text{m}^2$  by evaporation by using a shadow mask. The current–voltage (I–V) characterizations were performed by using an Agilent 4155C semiconductor parameter analyzer, respectively. The time-zero dielectric breakdown (TZDB) at various stress conditions was measured by the ramp-voltage breakdown test, and breakdown field distributions for  $\text{HfO}_2$  using  $\text{HfCl}_4$  and TDMAH were compared.

## RESULTS AND DISCUSSION

**$\text{HfO}_2$  Using  $\text{HfCl}_4$  on Graphene with Different Synthesis Processes.** To investigate nucleation and growth of ALD  $\text{HfO}_2$  depending on graphene synthesis methods, ALD  $\text{HfO}_2$  is deposited on both CVD and exfoliated graphene using  $\text{HfCl}_4$ . On exfoliated graphene, most of the ALD  $\text{HfO}_2$  nuclei grow along certain lines and a few islands form apart from 1D line deposits in Figure 1(a). On the contrary, although similar line shapes of ALD  $\text{HfO}_2$  are observed, many  $\text{HfO}_2$  nuclei have 0D dot shape on CVD graphene in Figure 1(b). Surface areal

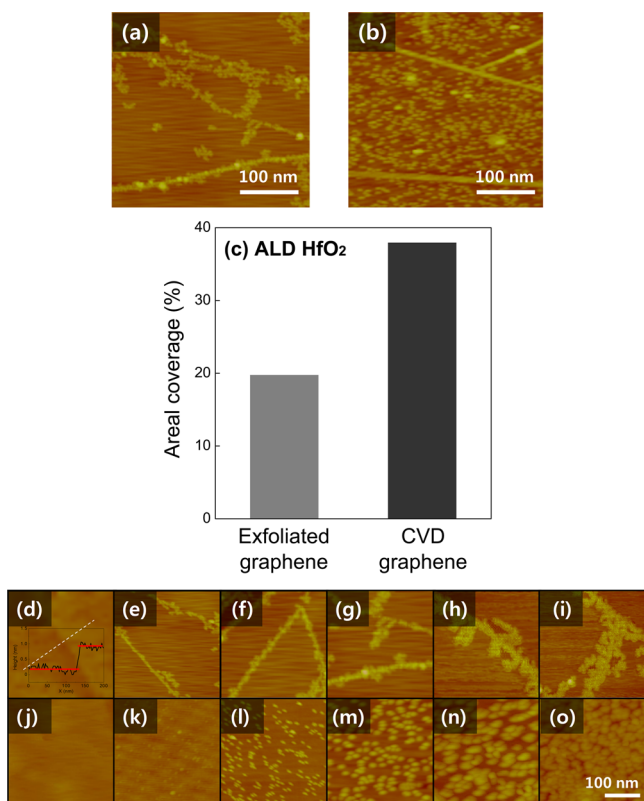


**Figure 1.** AFM images of 50 cycles ALD  $\text{HfO}_2$  on (a) exfoliated graphene and (b) CVD graphene and (c) their areal coverages. AFM images of  $\text{HfO}_2$  on graphene with 0, 10, 30, 50, 70, and 90 cycles. (d)–(i)  $\text{HfO}_2$  using  $\text{HfCl}_4$  on exfoliated graphene, (j)–(o)  $\text{HfO}_2$  using  $\text{HfCl}_4$  on CVD graphene. The inset of part (d) is the line spectrum of the height difference from the AFM image (d).

coverage of  $\text{HfO}_2$  on CVD graphene is 39%, two times larger than 19% on exfoliated graphene (Figure 1(c)). To understand different nucleation and growth characteristics, the morphological evolution of ALD  $\text{HfO}_2$  with the increasing ALD cycle number was investigated (Figure 1(d)–(i) for exfoliated graphene and Figure 1(j)–(o) for CVD graphene). ALD  $\text{HfO}_2$  was selectively formed with a line shape on exfoliated graphene after 10 cycles, while small  $\text{HfO}_2$  particle-like nuclei were observed on CVD graphene. With increasing the cycle number on exfoliated graphene, additional nucleation of  $\text{HfO}_2$  was rarely observed in the region where the line shape  $\text{HfO}_2$  did not exist, but ALD  $\text{HfO}_2$  grows and branches out from the pre-existing line shape  $\text{HfO}_2$  with an increasing cycle number on exfoliated graphene. In contrast, small particle-like  $\text{HfO}_2$  nuclei grow, and additional nucleation of  $\text{HfO}_2$  occurs on CVD graphene with increasing cycles.

The inset of Figure 1(d) shows a line profile along the white dashed line in Figure 1(d). There is a step across the exfoliated graphene surface of which the height is approximately 0.7 nm. Graphene prepared from exfoliation could have multilayers unlike single layer CVD graphene,<sup>40</sup> so that the step observed in Figure 1(d) is an edge of an upper graphene layer of multilayers. In addition, it was reported that step edges of HOPG have higher chemical reactivity than basal planes,<sup>5</sup> resulting in selective formation of ALD deposit on step edges.<sup>41</sup> Therefore, ALD  $\text{HfO}_2$  selectively nucleates on the step edges of multilayered exfoliated graphene, resulting in the formation of line shape  $\text{HfO}_2$ . In contrast to selective line growth on exfoliated graphene, particle shape ALD  $\text{HfO}_2$  forms on CVD graphene. Since ideal graphene does not have chemically available bonding for ALD nucleation, ALD growth cannot occur on the ideal surface of graphene. In addition, because CVD graphene is a single layer, there is no step edge. So, the formation of particle shape ALD  $\text{HfO}_2$  indicates that there are nonideal sites and surface species which initiate ALD nucleation. Interestingly, Figure 1(b) shows that a line shape  $\text{HfO}_2$  growth is observed besides particle shape nuclei in spite of there being no existence of a step edge on CVD graphene.

To investigate 1D growth of ALD  $\text{HfO}_2$  on CVD graphene in atomic scale, high-resolution scanning transmission electron microscopy (HR-STEM) was employed (Figure 2(a)–(e)). Figure 2(a) clearly shows that the ALD  $\text{HfO}_2$  grows along a line, and no growth occurs in other regions. Figure 2(b) and 2(c) are magnified HR-TEM images, and FFT patterns from A and B regions are denoted in Figure 2(a), respectively. Although the hexagonal crystal patterns of graphene are not clearly distinguishable by the eye in Figure 2(b) and 2(c), the FFT patterns show different orientations,  $111^\circ$  and  $126^\circ$ , obtained from A and B regions, respectively. Since FFT patterns mathematically are obtained from TEM images, they have the same relative orientations with real crystal structures.<sup>42</sup> Different crystal orientations are clearly observed in inverse FFT images in Figure 2(d) and 2(e) from Figure 2(b) and (c), respectively. Consistently, one orientation of hexagonal carbon rings is tilted by  $\sim 15^\circ$  from the other. This indicates that the two regions divided by the 1D ALD  $\text{HfO}_2$  line have different crystal orientations; in other words, they are different crystal grains, and ALD  $\text{HfO}_2$  is selectively formed along a grain boundary. The expected grain boundary is denoted by a red dashed line in Figure 2(a). Previously, grain boundaries have been reported as an arranged intrinsic defect in CVD graphene.<sup>43</sup> In our previous study, ALD Pt was selectively formed on line defects of CVD graphene, such as grain

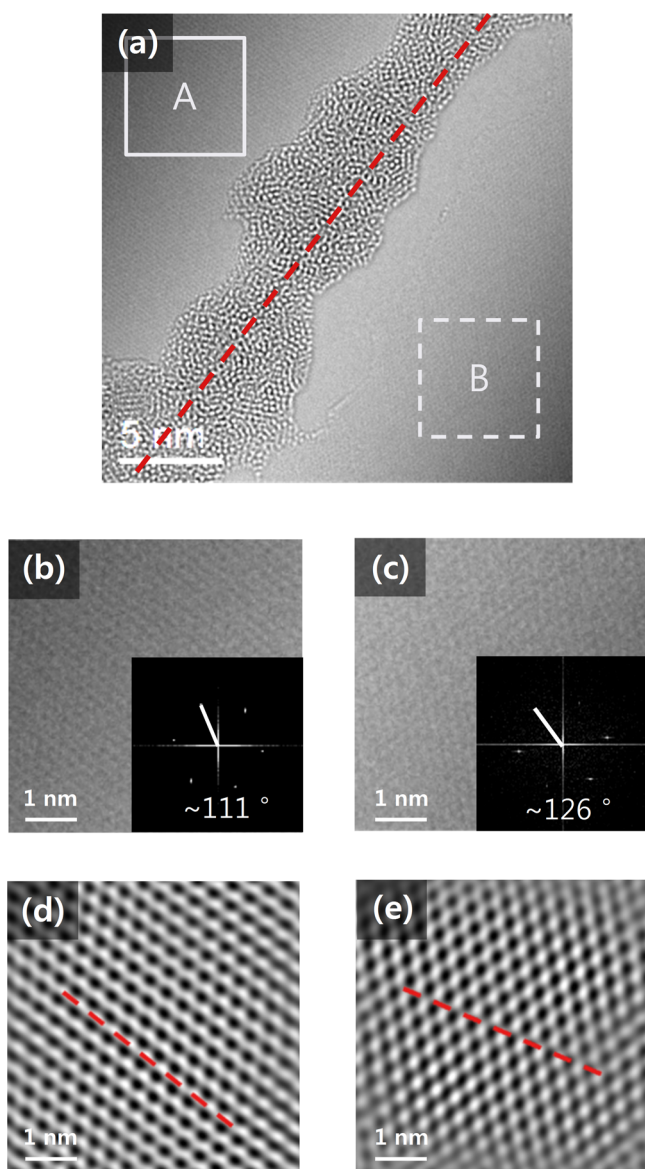


**Figure 2.** (a) TEM of HfO<sub>2</sub> 20 cycles on CVD graphene. Magnified images from (b) the white box of A and (c) the white box of B regions. Insets in (b) and (c), FFTs from each images. Inverse FFTs with masking from (b) and (c) and (d) and (e), respectively.

boundaries, since the defects have higher chemical reactivity than pristine sites.<sup>35</sup> Similarly, ALD HfO<sub>2</sub> nucleates along 1D grain boundaries, and it forms the 1D line shape after further increasing cycles.

Besides grain boundaries, the nucleation of ALD HfO<sub>2</sub> within a grain is due to nonideal sites and surface species. Two graphene samples were analyzed by XPS. Figure 3(a) and 3(b) show XPS fine scans of HOPG and CVD graphene in the C 1s core-level, respectively. The peaks at 284.8 and 285.6 eV correspond to C=C and C–C bonding of resonance structures of graphene, respectively.<sup>44</sup> The single and double bonds of C atoms observed in XPS are known to be sp<sup>2</sup> hybridization of carbons in the graphene surface which is the reason for the chemical inertness of the graphene surface due to no available dangling bond on the graphene surface.<sup>13</sup> On the other hand, the peaks at 286.3, 287.3, and 288.9 eV are assigned to epoxide (C–O), carbonyl (C=O), and carboxylic (O=C–O) groups, respectively. Peak area ratios of each deconvoluted peak to C=

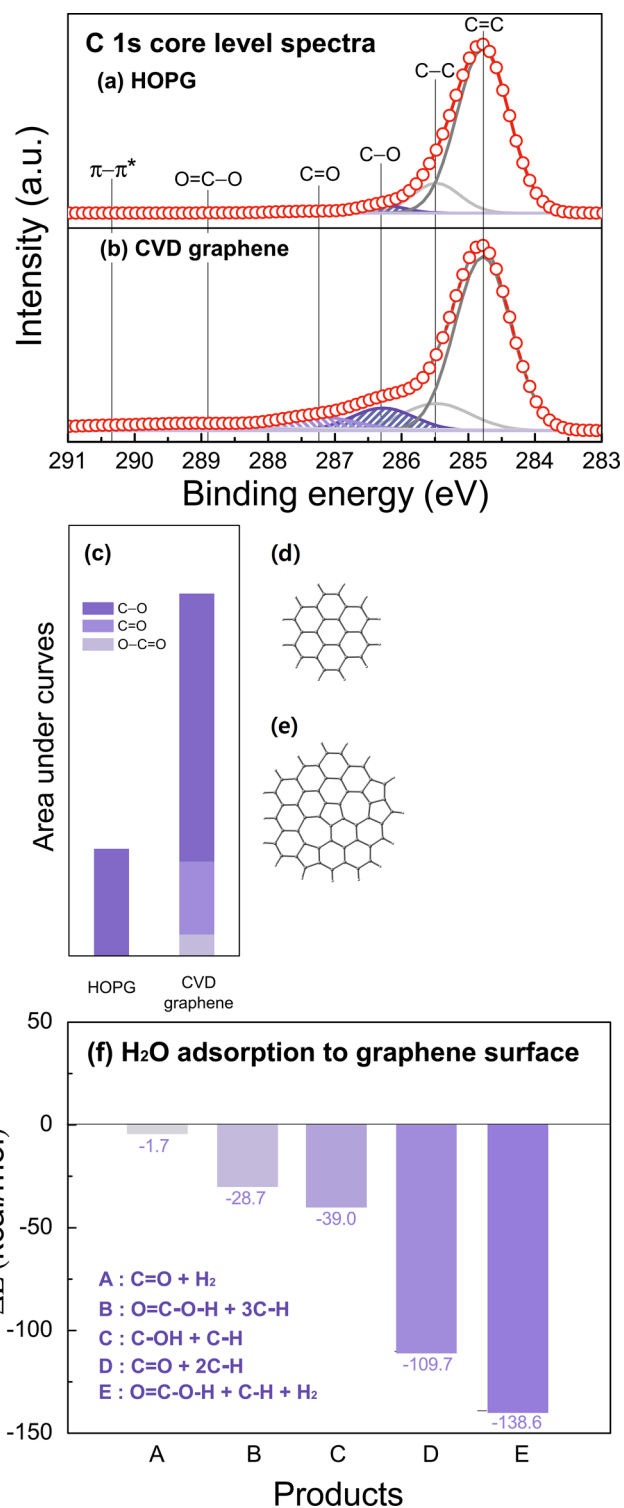


**Figure 3.** XPS of C 1s bonding configuration. (a) HOPG and (b) CVD graphene. (c) Normalized amounts of oxygen bonded to carbon in HOPG and CVD graphene. Two surface sites in graphene are modeled: (d) the pristine site and (e) the defect site. (f) The free energy difference of H<sub>2</sub>O chemisorption to the defect site and the pristine site from PBE0/SVP quantum chemical calculation. ΔE is the energy difference of adsorption energy to the defect site from adsorption energy to the pristine site.

C and C–C peak area are presented in Figure 3(c). Compared to HOPG, a larger amount of surface oxygen from C–O bonding is clearly observed on CVD graphene. In addition,

C=O and O=C–O bondings are only detected on CVD graphene.

Based on the growth mechanism on ALD HfO<sub>2</sub> by HfCl<sub>4</sub> and H<sub>2</sub>O, –OH species on a surface should be needed to initiate HfCl<sub>4</sub> precursor adsorption and subsequent HfO<sub>2</sub> growth.<sup>45</sup> In the previous reports, the carbon–oxygen bondings were detected on oxygen-functionalized graphene surface,<sup>6</sup> and they already contained –OH species or easily produced –OH species after exposure to water. Since the graphene surface is exposed to H<sub>2</sub>O during the ALD process, the C–O bondings are changed to –OH species, leading to the nucleation of ALD HfO<sub>2</sub>. C=O and O=C–O bondings could be also changed to –OH species after water exposure. Therefore, ALD HfO<sub>2</sub> more easily nucleates on CVD graphene than on exfoliated graphene due to a higher concentration of carbon–oxygen bondings. In addition, as-synthesized CVD graphene prior to transfer processes showed only C–O bonding without C=O and O=C=O, similar to HOPG.<sup>46</sup> After the transfer process, however, O=C–OH and C–OH were detected on CVD graphene because of using strong oxidants during the transfer process, such as moisture, oxygen, and acetone. In fact, an ideal graphene surface is chemically inert, so that it is hard for carbon–oxygen bondings that are generated from the reactions of oxidants and graphene to occur.<sup>47</sup> So, other sites, which are chemically reactive such as structural defects, are required to explain the formation of carbon–oxygen bondings.

Calculating adsorption energy of oxidants on graphene surfaces provides the quantitative estimation of the formation of carbon–oxygen bondings on different surfaces. The adsorption of water is numerically investigated by computational calculations. Two different surface sites of graphene are modeled: one is a pristine site and the other is a defect site as shown in Figure 3(d) and (e), respectively. The calculations of each adsorption were performed, and the results are presented in Figure 3(f). The reaction between graphene and H<sub>2</sub>O produces various products including C–OH + H<sub>2</sub>, C=O + H<sub>2</sub>, C=O + 2C–H, O=C–OH + 3C–H, and O=C–OH + C–H + H<sub>2</sub>. The free energy difference on the defect site and the pristine site shows a negative value for all the products, indicating that the energetics for H<sub>2</sub>O adsorption on graphene are much more favorable on the defect site than the pristine site. Moreover, these calculations result in that H<sub>2</sub>O adsorption produces C–OH, C=O, and O=C–OH bondings on defect sites consistent with our observations from XPS results. In addition, other evidence for high defect density of CVD graphene were observed in Raman and TEM results (see Figures S1 and S4 in the Supporting Information). Since H<sub>2</sub>O more favorably chemisorbs on the defect site than on the pristine site, surface adsorbates can be formed easily on defect sites than on pristine sites, leading to a higher nucleation rate of ALD HfO<sub>2</sub> on CVD graphene. Therefore, besides 1D selective growth on grain boundaries, a larger amount of ALD HfO<sub>2</sub> nuclei are formed on CVD graphene than that on exfoliated graphene. The H<sub>2</sub>O adsorption can occur during both the graphene transfer steps and counter reactant exposure of ALD. Since ALD reactant exposure is performed at elevated temperature unlike the transfer process at room temperature, it is likely that the oxidation and generations of oxygen species are dominant during the ALD reactant exposure process.<sup>48</sup>

In addition, defects might be generated during the deposition process. One is the defect generation by the direct reaction between graphene and precursor and/or H<sub>2</sub>O. From the DFT

calculation, however, we observed the precursor and reactant unfavorably react on the pristine sites of graphene. So, it is hard to generate defects by direct reaction between graphene and precursor/reactant during the deposition process. The other is reaction between graphene and byproducts from the ALD reaction, such as HCl. However, HCl physisorbed on graphene is easily desorbed from surface rather than involved in defect generation reactions.<sup>45</sup> Also, it was reported that HCl could not etch out graphene.<sup>49,50</sup> Also, the constant nucleation rate with increasing ALD cycle number indicates that there is no additional generation of defects during the ALD process (see Figure S2 in the Supporting Information). In addition, Raman results on graphene before and after HfO<sub>2</sub> ALD clearly show that there is no notable difference in the D band (see Figures S1(f), S7(a), and S7(b) in the Supporting Information). Therefore, based on indirect and direct evidence it can be concluded that no defect is generated during the ALD process.

#### HfO<sub>2</sub> Using HfCl<sub>4</sub> and TDMAH on CVD Graphene.

Generally, metal–organic precursors have been more widely used for HfO<sub>2</sub> ALD than chlorine-based precursors due to their negative effects, such as a corrosion of reactor and chlorine residues.<sup>51,52</sup> In addition, selection of the precursor strongly affects growth characteristics of ALD, so that exploring the precursor is important to fabricate a suitable high-k layer for graphene-based devices. So, ALD HfO<sub>2</sub> on graphene was investigated by using a metal–organic precursor, TDMAH. In Figure 4(a)–(e), the apparent areal coverage of ALD HfO<sub>2</sub> using TDMAH is smaller than that using HfCl<sub>4</sub> shown in Figure 1. For quantitative discussion, the areal coverage and number of nuclei measured from AFM images are plotted in Figure 4(f) and 4(g), respectively, at various cycle numbers. With increasing ALD cycles up to 90, higher areal coverage of HfCl<sub>4</sub> (75%) is observed than that of TDMAH (34%). Over 90 cycles, the areal coverages of HfO<sub>2</sub> continuously increased with different change rates and reached 100% of coverage at 120 cycles for HfCl<sub>4</sub> and 230 cycles for TDMAH (see Figure S6(f) in the Supporting Information). Of all the cycle numbers studied, the areal coverage of HfO<sub>2</sub> on graphene is much smaller than that on Si and SiO<sub>2</sub> (see Figure S8(a) in the Supporting Information). Because the density of the reactive sites on Si and SiO<sub>2</sub> surfaces for ALD nucleation, such as the –OH group, is much greater than the density of defect sites on graphene, the nucleation rate on Si and SiO<sub>2</sub> is much faster than that on graphene, leading to high surface coverage.

The number density of HfO<sub>2</sub> nuclei gradually increases in both HfCl<sub>4</sub> and TDMAH plots, but it decreases over a certain cycle number due to the coalescence of nuclei. The starting cycle number of coalescence for HfCl<sub>4</sub> is over 30 cycles shorter than 50 cycles for TDMAH. The nucleation rate of ALD HfO<sub>2</sub> extracted from the slope of the plots up to 30 cycles is 3.1/cycle for HfCl<sub>4</sub>, higher than 2.2/cycle for TDMAH. Since the ALD process was performed under the same conditions except for the Hf precursor, the higher nucleation rate for HfCl<sub>4</sub> is ascribed to the higher reactivity of HfCl<sub>4</sub> with graphene than that of TDMAH. The maximum value in the number of nuclei in Figure 4(g) can be translated to density of nucleation sites on graphene and the densities  $1.08 \times 10^{11} \text{ cm}^{-2}$  for HfCl<sub>4</sub> and  $9.33 \times 10^{10} \text{ cm}^{-2}$  for TDMAH. In addition, a density of graphene defect which is a main nucleation site for ALD can be extracted by using the intensity ratio of D to G peaks<sup>53,54</sup> from Raman (see Supporting Information Figure S1(f)), and that is  $2.04 \times 10^{10} \text{ cm}^{-2}$ . The differences are not too large, but they can be explained by several reasons. Although both HfCl<sub>4</sub> and

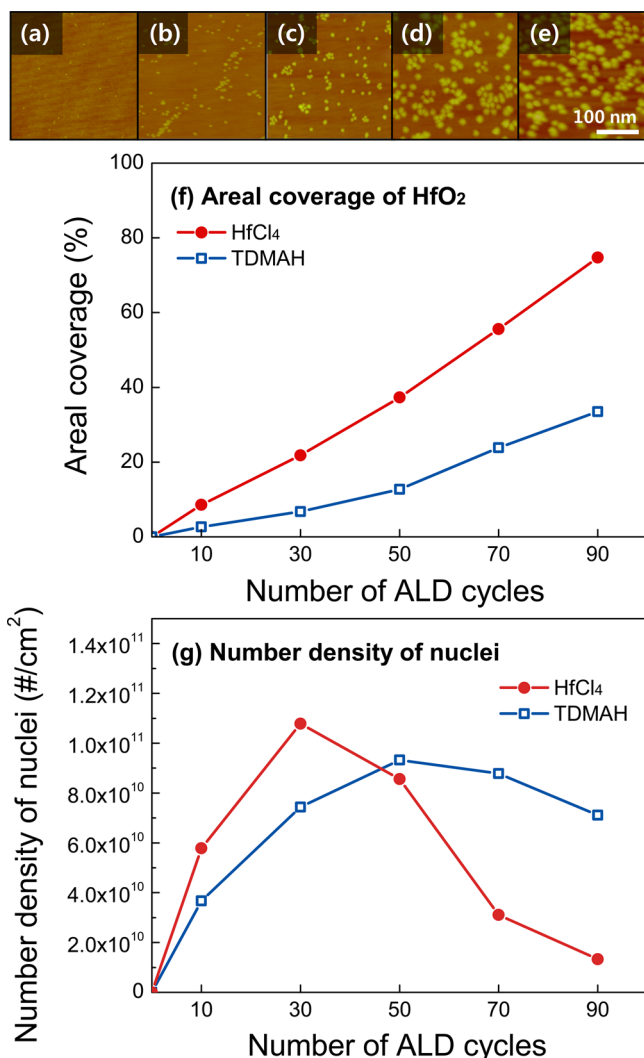


**Figure 4.** (a)–(e) AFM images of HfO<sub>2</sub> by TDMAH on CVD graphene with 10, 30, 50, 70, and 90 cycles. (f) Areal coverage and (g) density of nuclei of HfO<sub>2</sub> by using HfCl<sub>4</sub> and TDMAH on CVD graphene from the AFM data of Figure 1 (g)–(l) and parts (a)–(e) of this figure.

TDMAH nucleate dominantly on defect sites, there still exists the possibility of growth on the pristine site and C–OH since HfCl<sub>4</sub> adsorbs endothermically both on the pristine site and C–OH, while TDMAH does on C–OH. In addition, there exist errors in the nuclei counting in AFM images and the calculation of defect density from Raman spectra.

In the previous section, we observed HfO<sub>2</sub> growth using HfCl<sub>4</sub> due to the existence of C–OH bonding on the defect sites of the CVD graphene. HfCl<sub>4</sub> and TDMAH adsorptions on the C–OH site are quantum-chemically calculated, and the results are denoted by a red color in Figure 5(a) for HfCl<sub>4</sub> and Figure 5(b) for TDMAH. HfCl<sub>4</sub> more favorably physisorbs initially on the C–OH site (–34.6 kcal/mol) than TDMAH (–9.5 kcal/mol) at the initial physisorption state. However, there is a larger activation barrier for transition from initial physisorption to the final product in the HfCl<sub>4</sub> reaction pathway (21.7 kcal/mol) than that in TDMAH (13.6 kcal/mol), indicating that HfCl<sub>4</sub> adsorption on the C–OH site is less favorable than TDMAH. Moreover, the activation energy of TDMAH at the final product state is –21.5 kcal/mol, smaller than that of HfCl<sub>4</sub>, –17.5 kcal/mol. Therefore, although both

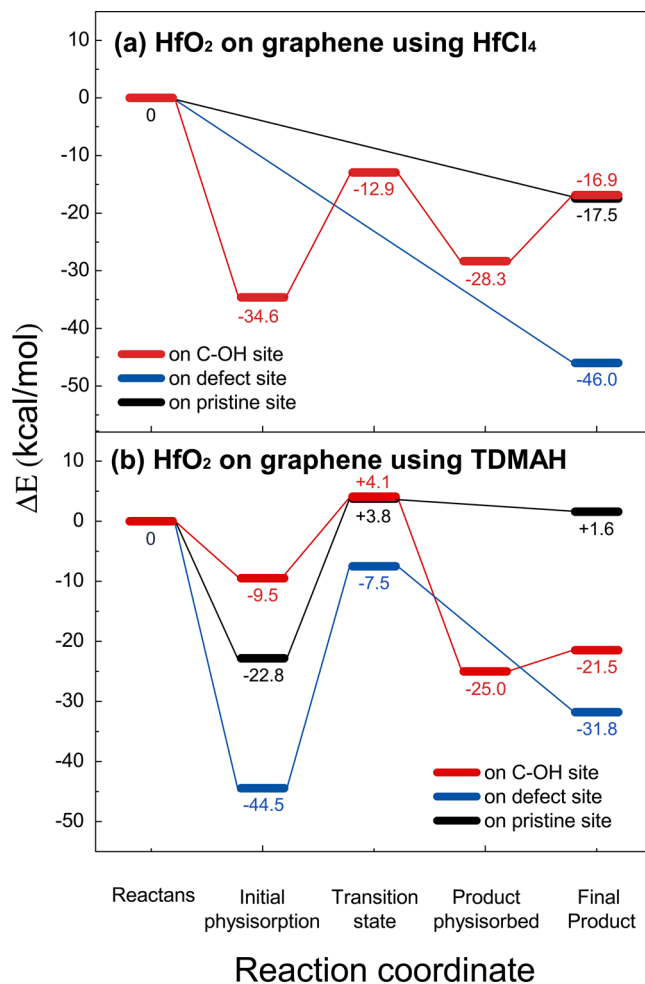


**Figure 5.** PBE0/SVP quantum chemical calculation of HfO<sub>2</sub> using (a) HfCl<sub>4</sub> and (b) TDMAH on C–OH, the pristine site, and the defect site of graphene.

HfCl<sub>4</sub> and TDMAH adsorptions on the C–OH site are favorable, the adsorption of TDMAH is more favorable than HfCl<sub>4</sub>.

Interestingly, ALD HfO<sub>2</sub> using HfCl<sub>4</sub> shows higher areal coverage than that using TDMAH (Figure 4(f)), which shows an inconsistency between the experimental observation and the calculation results. So, other nucleation sites for ALD HfO<sub>2</sub>, such as the pristine site and the defect site without oxygen species were considered as denoted by black and blue colors in Figure 5(a) and Figure 5(b), respectively. For HfCl<sub>4</sub>, no viable reaction states and no energy barrier are found to the final product state. This means that the HfCl<sub>4</sub> adsorption process is physisorption rather than chemisorption by changing its tetrahedron structure at the final product state (see Figure S9 in the Supporting Information). The activation energy of HfCl<sub>4</sub> physisorption on defect sites is –46 kcal/mol, much smaller than that on pristine sites, –17.5 kcal/mol in Figure 6(a). Although the activation energy of TDMAH adsorption on defect sites is very small down to –31.8 kcal/mol, there is an energy barrier as high as 37 kcal/mol between the initial physisorption and the final product state (Figure 5(b)). On the pristine site, the energy barrier is also observed, and the activation energy at the final product state is a positive value in TDMAH adsorption. In contrast to HfCl<sub>4</sub>, TDMAH is chemisorbed on pristine and defect sites by breaking strong

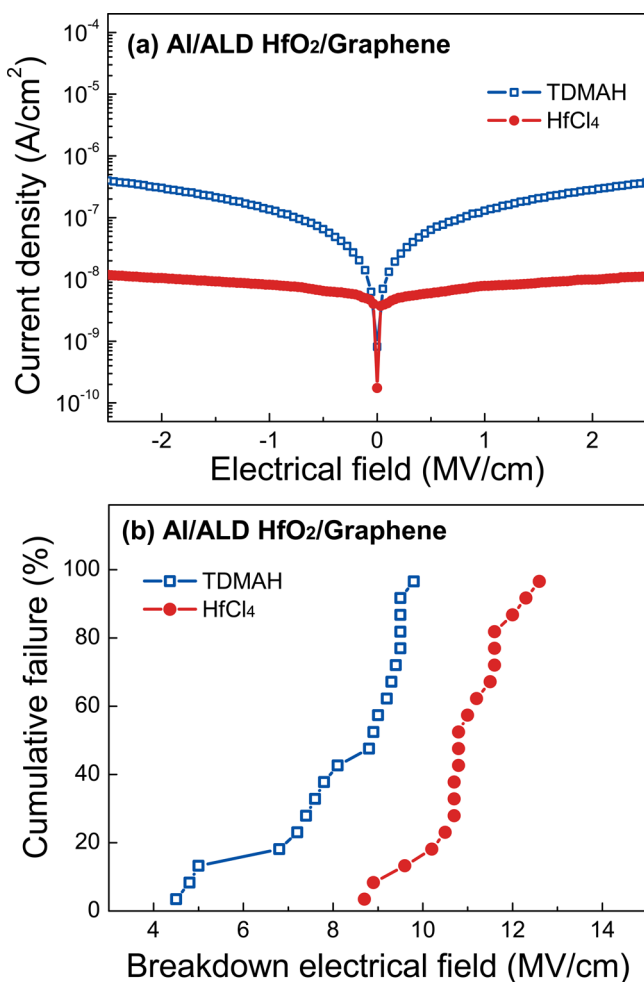


**Figure 6.** (a) I–V curves and (b) cumulative failure as a function of the breakdown electrical field. MIG capacitors with ALD HfO<sub>2</sub> using HfCl<sub>4</sub> and TDMAH deposited on CVD graphene for 1000 cycles were fabricated.

C–C or C=C bonding of graphene, resulting in C–Hf bonding at the transition state (see Figure S9 in the [Supporting Information](#)). From these calculations, two important pieces of information are obtained. Both TDMAH and HfCl<sub>4</sub> can be adsorbed on defect sites, even on the pristine site for HfCl<sub>4</sub>, and the adsorption on defect sites is much more favorable than on the pristine sites. The other one is that HfCl<sub>4</sub> adsorption on the defect site occurs through physisorption without transition states instead of chemisorption. So, the higher areal coverage of ALD HfO<sub>2</sub> using HfCl<sub>4</sub> can be attributed to contributions of HfCl<sub>4</sub> physisorption on pristine and defect sites to HfO<sub>2</sub> nucleation.

The growth of ALD HfO<sub>2</sub> on graphene could be changed by varying other process parameters, such as growth temperature and oxidant. ALD HfO<sub>2</sub> process windows in which growth per cycles (GPCs) are constant due to the self-saturated ALD reaction are 130–250 °C for HfCl<sub>4</sub> and 175–250 °C for TDMAH (see Figure S10 in the [Supporting Information](#)). At lower temperature than the ALD windows, precursor molecules can physisorb on the surface through thermal condensation instead of chemisorbing, resulting in an increase of GPC. Thus, although ALD HfO<sub>2</sub> noncontinuously grows on graphene with low GPC within the ALD window, a continuous HfO<sub>2</sub> may form at lower temperature. In addition, the different adsorption

behavior and growth characteristics between HfCl<sub>4</sub> and TDMAH observed in the ALD window can be changed at lower temperature because HfO<sub>2</sub> films are not formed through the self-saturated reactions which cause the difference. However, the HfO<sub>2</sub> deposited at lower temperature than the ALD window has a low film quality, such as low dielectric constant and high impurity concentration due to an incomplete reaction. So, in other reports, the continuous growth of the low quality ALD layer was just utilized for a seed layer, and the high quality ALD film was deposited on that seed layer to fabricate the continuous high-k layer of graphene-based devices.<sup>13,55</sup> The role of oxidants is also important. The previous DFT study of O<sub>3</sub>-ALD Al<sub>2</sub>O<sub>3</sub> on graphene has shown that O<sub>3</sub> physisorbs on graphene and initiates nucleation of Al<sub>2</sub>O<sub>3</sub> during the ALD process.<sup>56,57</sup> In the following study, a uniform Al<sub>2</sub>O<sub>3</sub> layer is formed by physisorbed O<sub>3</sub> in contrast to the nonuniform growth of Al<sub>2</sub>O<sub>3</sub> by H<sub>2</sub>O. However, the O<sub>3</sub> oxidant might generate an undesired p-type doping effect for graphene,<sup>56</sup> so careful control of O<sub>3</sub> is needed.

Different nucleation and growth mechanism significantly affect insulating properties of HfO<sub>2</sub> for a graphene-based device. Figure 6(a) shows leakage current densities between Al top electrode and graphene. Leakage current density of HfO<sub>2</sub> at –1 MV of the electrical field is  $8.22 \times 10^{-9}$  A/cm<sup>2</sup> for HfCl<sub>4</sub>, almost 17 times lower than  $1.36 \times 10^{-7}$  A/cm<sup>2</sup> for TDMAH. Figure 6(b) shows cumulative failure as a function of a breakdown electrical field. Compared to HfCl<sub>4</sub>, a lower breakdown electrical field was observed in that by using TDMAH. In contrast to HfCl<sub>4</sub>, several samples by using TDMAH showed a weak breakdown property below 5 MV/cm of the electrical field. These results indicate that ALD HfO<sub>2</sub> by using HfCl<sub>4</sub> is a better insulator than that by using TDMAH. Electrical properties can be explained by the correlation of nucleation and growth of HfO<sub>2</sub> depending on Hf precursors. The nucleation rate and the number of nuclei are higher in ALD HfO<sub>2</sub> using HfCl<sub>4</sub> than that using TDMAH, leading to the faster coalescence as shown in Figure 4(g). Surface roughness of thin film is strongly affected by initial nucleation and coalescence, and a film with high nucleation rate and fast coalescence has smoother surface morphology than that with low nucleation rate and slow coalescence.<sup>58</sup> In our experiment, 1000 cycles of HfO<sub>2</sub> using HfCl<sub>4</sub> produced a smoother surface than that using TDMAH (see Figure S11 in the [Supporting Information](#)). The rough surface forms a rough interface between the top Al electrode and HfO<sub>2</sub>, leading to electric field enhancement due to geometrical effects.<sup>59</sup> The electric field is increased at the region where the thickness of HfO<sub>2</sub> is relatively thin, resulting in the electron emission.<sup>60</sup> The emitted electrons to oxide layer generate holes at the anode. When the hole concentration is over a critical point, accumulated holes tunnel into the oxide layers, leading to an intrinsic breakdown.<sup>61</sup> So, the electric field enhancement by effects of roughness lowers the electric breakdown field of insulating films. In addition, the average grain size of ALD HfO<sub>2</sub> can affect the deterioration of the insulating property. Due to the high nucleation rate and fast coalescence, the average grain size of ALD HfO<sub>2</sub> using HfCl<sub>4</sub> is larger than that using TDMAH. At 1000 cycles, the average grain size of ALD HfO<sub>2</sub> using HfCl<sub>4</sub> and TDMAH are  $4.25 \times 10^5$  nm<sup>2</sup> and  $8.73 \times 10^4$  nm<sup>2</sup>, respectively (see Figure S11(a) and S11(b) in the [Supporting Information](#)). The large ALD HfO<sub>2</sub> grain using HfCl<sub>4</sub> can more densely cover the graphene surface than that using TDMAH, so that the size of pinholes which are the dominant leakage path is smaller (see Figure

S11(c) and S11(d) in the [Supporting Information](#)). Thus, the ALD HfO<sub>2</sub> using HfCl<sub>4</sub> is more suitable for graphene-based electrical devices than that using TDMAH.

## CONCLUSIONS

In this research, we investigated growth characteristics of HfO<sub>2</sub> on exfoliated and CVD graphene by using two Hf precursors, TDMAH and HfCl<sub>4</sub>. On exfoliated graphene, 1D growth of ALD HfO<sub>2</sub> using HfCl<sub>4</sub> along the step edges was observed. On the contrary, 0D HfO<sub>2</sub> nucleated on CVD graphene together with 1D HfO<sub>2</sub>, due to the existence of nonideal sites. Compared to exfoliated graphene, CVD graphene showed a larger amount of chemically reactive defect sites, which are effective nucleation sites for ALD HfO<sub>2</sub>. ALD HfO<sub>2</sub> by using TDMAH on CVD graphene showed much more unfavorable nucleation and growth than that by using HfCl<sub>4</sub>. From the quantum chemical calculation, it is revealed that the higher areal coverage of ALD HfO<sub>2</sub> using HfCl<sub>4</sub> than TDMAH is attributed to HfCl<sub>4</sub> physisorption on pristine and defect sites on graphene. From the electrical property measurements, ALD HfO<sub>2</sub> using HfCl<sub>4</sub> showed superior properties, such as lower leakage currents and breakdown electric field, to that using TDMAH due to smoother and denser surface morphology from the higher nucleation rate and larger number of HfO<sub>2</sub> nuclei during initial growth. It should be noted that our findings from comparative research of ALD HfO<sub>2</sub> would be significant fundamentally and practically for fabrication of graphene-based electronic devices.

## ASSOCIATED CONTENT

### Supporting Information

The Supporting Information is available free of charge on the ACS Publications website at DOI: [10.1021/acs.chemmater.5b01226](https://doi.org/10.1021/acs.chemmater.5b01226).

Technical information and Figures S1–S11 ([PDF](#))

## AUTHOR INFORMATION

### Corresponding Authors

\*E-mail: [hyungjun@yonsei.ac.kr](mailto:hyungjun@yonsei.ac.kr) (H.K.).

\*E-mail: [hbrlee@incheon.ac.kr](mailto:hbrlee@incheon.ac.kr) (H.-B.-R.L.).

### Author Contributions

I.-K.O., H.K., and H.-B.-R.L. conceived the research. H.K. and H.-B.-R.L. supervised the research. J.T. calculated activation energy and energetic of reaction pathways during the ALD process by quantum chemical calculations. H.J. investigated surface morphologies of ALD HfO<sub>2</sub> on graphene with increasing cycles by AFM. K.K., M.J.L., and Z.L. analyzed ALD HfO<sub>2</sub> on graphene by the atomic scale image by TEM. S.-K.L. and J.-H.A. prepared CVD graphene substrate and analyzed vibrational energy states by Raman. C.W.L. analyzed the chemical composition of the graphene surface by XPS. I.-K.O. fabricated and measured the electrical properties of graphene-based devices. K.K. advised the growth characteristics of ALD HfO<sub>2</sub> on graphene. All authors contributed to the writing and revising of the manuscript.

### Notes

The authors declare no competing financial interest.

## ACKNOWLEDGMENTS

This work was supported by the Industrial Strategic Technology Development Program (10041926, Development of high-density plasma technologies for thin-film deposition of

nanoscale semiconductor and flexible display processing), funded by the Ministry of Knowledge Economy (MKE, Korea), by the Basic Science Research Program through the National Research Foundation of Korea (NRF) funded by the Ministry of Education (2014R1A1A2059845), by the Korea Evaluation Institute of Industrial Technology (KEIT) funded by the Ministry of Trade, Industry and Energy (MOTIE) (Project No. 10050296, Large scale (Over 8") synthesis and evaluation technology of 2-dimensional chalcogenides for next generation electronic devices), and by the National Research Foundation of Korea (NRF) grant funded by the Korea government (MSIP) (No. NRF-2014R1A2A1A11052588).

## REFERENCES

- (1) Morozov, S. V.; Novoselov, K. S.; Katsnelson, M. I.; Schedin, F.; Elias, D. C.; Jaszczak, J. A.; Geim, A. K. Giant Intrinsic Carrier Mobilities in Graphene and Its Bilayer. *Phys. Rev. Lett.* **2008**, *100*, 16602.
- (2) Liao, L.; Duan, X. Graphene–dielectric integration for graphene transistors. *Mater. Sci. Eng., R* **2010**, *70*, 354–370.
- (3) Ni, Z. H.; Wang, H. M.; Ma, Y.; Kasim, J.; Wu, Y. H.; Shen, Z. X. Tunable stress and controlled thickness modification in graphene by annealing. *ACS Nano* **2008**, *2*, 1033–1039.
- (4) Kim, H. Atomic layer deposition of metal and nitride thin films: Current research efforts and applications for semiconductor device processing. *J. Vac. Sci. Technol., B: Microelectron. Process. Phenom.* **2003**, *21*, 2231.
- (5) Wang, X. R.; Tabakman, S. M.; Dai, H. Atomic layer deposition of metal oxides on pristine and functionalized graphene. *J. Am. Chem. Soc.* **2008**, *130*, 8152–8153.
- (6) Lee, B.; Park, S.-Y.; Kim, H.-C.; Cho, K.; Vogel, E. M. Conformal Al<sub>2</sub>O<sub>3</sub> dielectric layer deposited by atomic layer deposition for graphene-based nanoelectronics. *Appl. Phys. Lett.* **2008**, *92*, 203102.
- (7) Xuan, Y.; Wu, Y. Q.; Shen, T.; Qi, M.; Capano, M. A.; Cooper, J. A.; Ye, P. D. Top-gated graphene field-effect-transistors formed by decomposition of SiC. *Appl. Phys. Lett.* **2008**, *92*, 013101.
- (8) Speck, F.; Ostler, M.; Röhr, J.; Emtsev, K. V.; Hundhausen, M.; Ley, L.; Seyller, T. Atomic layer deposited aluminum oxide films on graphite and graphene studied by XPS and AFM. *Phys. Status Solidi C* **2010**, *7*, 398–401.
- (9) Lee, B.; Mordí, G.; Park, T.; Goux, L.; Chabal, Y. J.; Cho, K.; Vogel, E. M.; Kim, M.; Colombo, L.; Wallace, R. M.; Kim, J. Atomic-layer-deposited Al<sub>2</sub>O<sub>3</sub> as gate dielectrics for graphene-based devices. *J. ECS Trans.* **2009**, *19* (5), 225–230.
- (10) Pirkle, A.; McDonnell, S.; Lee, B.; Kim, J.; Colombo, L.; Wallace, R. M. The effect of graphite surface condition on the composition of Al<sub>2</sub>O<sub>3</sub> by atomic layer deposition. *Appl. Phys. Lett.* **2010**, *97*, 082901.
- (11) Dlubak, B.; Kidambi, P. R.; Weatherup, R. S.; Hofmann, S.; Robertson, J. Substrate-assisted nucleation of ultra-thin dielectric layers on graphene by atomic layer deposition. *Appl. Phys. Lett.* **2012**, *100*, 173113.
- (12) Lupina, G.; Lukosius, M.; Kitzmann, J.; Dabrowski, J.; Wolff, A.; Mehr, W. Nucleation and growth of HfO<sub>2</sub> layers on graphene by chemical vapor deposition. *Appl. Phys. Lett.* **2013**, *103*, 183116.
- (13) Zheng, L.; Cheng, X.; Cao, D.; Wang, Z.; Xu, D.; Xi, C.; Shen, L.; Yuehui, Y. HfO<sub>2</sub> dielectric film growth directly on graphene by H<sub>2</sub>O-based atomic layer deposition. *J. Vac. Sci. Technol., A* **2014**, *32*, 01A103.
- (14) Shen, T.; Gu, J. J.; Xu, M.; Wu, Y. Q.; Bolen, M. L.; Capano, M. A.; Engel, L. W.; Ye, P. D. Observation of quantum-Hall effect in gated epitaxial graphene grown on SiC (0001). *Appl. Phys. Lett.* **2009**, *95*, 172105.
- (15) Chen, Q.; Huang, H.; Chen, W.; Wee, A. T. S.; Feng, Y. P.; Chai, J. W.; Zhang, Z.; Pan, J. S.; Wang, S. J. In situ photoemission spectroscopy study on formation of HfO<sub>2</sub> dielectrics on epitaxial graphene on SiC substrate. *Appl. Phys. Lett.* **2010**, *96*, 072111.

- (16) Robinson, J. A.; LaBella, M.; Trumbull, K. A.; Weng, X. J.; Cavelero, R.; Daniels, T.; Hughes, Z.; Hollander, M.; Fanton, M.; Snyder, D. Epitaxial graphene materials integration: effects of dielectric overlayers on structural and electronic properties. *ACS Nano* **2010**, *4*, 2667–2672.
- (17) Pirkle, A.; Wallace, R. M.; Colombo, L. In situ studies of Al<sub>2</sub>O<sub>3</sub> and HfO<sub>2</sub> dielectrics on graphite. *Appl. Phys. Lett.* **2009**, *95*, 133106.
- (18) Kim, S.; Nah, J.; Jo, I.; Shahrjerdi, D.; Colombo, L.; Yao, Z.; Tutuc, E.; Banerjee, S. K. Realization of a high mobility dual-gated graphene field effect transistor with Al<sub>2</sub>O<sub>3</sub> dielectric. *Appl. Phys. Lett.* **2009**, *94*, 062107.
- (19) Pirkle, A.; Chabal, Y. J.; Colombo, L.; Wallace, R. M. In-situ Studies of High- $\kappa$  Dielectrics for Graphene-Based Device. *ECS Trans.* **2009**, *19*, 215–224.
- (20) Lee, B. K.; Park, S. Y.; Kim, H. C.; Cho, K.; Vogel, E. M.; Kim, M. J.; Wallace, R. M.; Kim, J. Y. *Appl. Phys. Lett.* **2008**, *92*, 203102.
- (21) Lee, B.; Mordí, G.; Kim, M. J.; Chabal, Y. J.; Vogel, E. M.; Wallace, R. M.; Cho, K. J.; Colombo, L.; Kim, J. *Appl. Phys. Lett.* **2010**, *97*, 043107.
- (22) Shin, W. C.; Bong, J. H.; Choi, S.-Y.; Cho, B. J. Functionalized graphene as an ultrathin seed layer for the atomic layer deposition of conformal high-k dielectrics on graphene. *ACS Appl. Mater. Interfaces* **2013**, *5* (22), 11515–11519.
- (23) Lin, Y. M.; Jenkins, K. A.; Valdes-Garcia, A.; Small, J. P.; Farmer, D. B.; Avouris, P. Operation of graphene transistors at gigahertz frequencies. *Nano Lett.* **2009**, *9*, 422–426.
- (24) Farmer, D. B.; Chiu, H. Y.; Lin, Y. M.; Jenkins, K. A.; Xia, F. N.; Avouris, P. Utilization of a buffered dielectric to achieve high field-effect carrier mobility in graphene transistors. *Nano Lett.* **2009**, *9*, 4474–4478.
- (25) Lin, Y. M.; Dimitrakopoulos, C.; Jenkins, K. A.; Farmer, D. B.; Chiu, H. Y.; Grill, A.; Avouris, P. 100-GHz transistors from wafer-scale epitaxial graphene. *Science* **2010**, *327*, 662–662.
- (26) Alaboson, J. M. P.; Wang, Q. H.; Emery, J. D.; Lipson, A. L.; Bedzyk, M. J.; Elam, J. W.; Pellin, M. J.; Hersam, M. C. Seeding atomic layer deposition of high-k dielectrics on epitaxial graphene with organic self-assembled monolayers. *ACS Nano* **2011**, *5* (6), 5223–5232.
- (27) Novoselov, K. S.; Geim, A. K.; Morozov, S. V.; Jiang, D.; Zhang, Y.; Dubonos, S. V.; Grigorieva, I. V.; Firsov, A. A. Electric field effect in atomically thin carbon films. *Science* **2004**, *306*, 666.
- (28) Lee, S.-K.; Jang, H. Y.; Jang, S.; Choi, E.; Hong, B. H.; Lee, J.; Park, S.; Ahn, J.-H. All graphene-based thin film transistors on flexible plastic substrates. *Nano Lett.* **2012**, *12*, 3472–3476.
- (29) Regan, W.; Alem, N.; Alemán, B.; Geng, B.; Girit, Ç.; Maserati, L.; Wang, F.; Crommie, M.; Zettl, A. A direct transfer of layer-area graphene. *Appl. Phys. Lett.* **2010**, *96*, 113102.
- (30) Perdew, J. P.; Burke, K.; Ernzerhof, M. Generalized gradient approximation made simple. *Phys. Rev. Lett.* **1996**, *77*, 3865.
- (31) Adamo, C.; Barone, V. Toward reliable density functional methods without adjustable parameters: The PBE0 model. *J. Chem. Phys.* **1999**, *110*, 6158.
- (32) Schafer, A.; Horn, H.; Ahlrichs, R. Fully optimized contracted Gaussian basis sets for atoms Li to Kr. *J. Chem. Phys.* **1992**, *97*, 2571.
- (33) Schafer, A.; Huber, C.; Ahlrichs, R. Fully optimized contracted Gaussian basis sets of triple zeta valence quality for atoms Li to Kr. *J. Chem. Phys.* **1994**, *100*, 5829.
- (34) Andrae, D.; Häußermann, U.; Dolg, M.; Stoll, H.; Preuß, H. Energy-adjusted ab initio pseudopotentials for the second and third row transition elements. *Theor. Chim. Acta* **1990**, *77*, 123.
- (35) Kim, K.; Lee, H.-B.-R.; Johnson, R. W.; Tanskanen, J. T.; Liu, N.; Kim, M.-G.; Pang, C.; Ahn, C.; Bent, S. F.; Bao, Z. Selective metal deposition at graphene line defects by atomic layer deposition. *Nat. Commun.* **2014**, *5*, 4781.
- (36) Weigend, F.; Häser, M. Theor. RI-MP2: first derivatives and global consistency. *Theor. Chem. Acc.* **1997**, *97*, 331.
- (37) Weigend, F.; Häser, M.; Patzelt, H.; Ahlrichs, R. RI-MP2: optimized auxiliary basis sets and demonstration of efficiency. *Chem. Phys. Lett.* **1998**, *294*, 143.
- (38) Ahlrichs, R.; Bär, M.; Häser, M.; Horn, H.; Kölmel, C. Electronic structure calculations on workstation computers: The program system turbomole. *Chem. Phys. Lett.* **1989**, *162*, 165.
- (39) Weigend, F.; Ahlrichs, R. Balanced basis sets of split valence, triple zeta valence and quadruple zeta valence quality for H to Rn: design and assessment of accuracy. *Phys. Chem. Chem. Phys.* **2005**, *7*, 3297.
- (40) Shahil, K. M. F.; Balandin, A. A. Graphene–multilayer graphene nanocomposites as highly efficient thermal interface materials. *Nano Lett.* **2012**, *12*, 861–867.
- (41) Lee, H.-B.-R.; Baeck, S. H.; Jaramillo, T. F.; Bent, S. F. Growth of Pt nanowires by atomic layer deposition on highly ordered pyrolytic graphite. *Nano Lett.* **2013**, *13*, 457–463.
- (42) Conte, S. D.; de Boor, C. *Elementary Numerical Analysis*, 3rd ed.; McGraw Hill, Inc.: New York, 1980.
- (43) Yazyev, O. V.; Louie, S. G. Topological defects in graphene: Dislocations and grain boundaries. *Phys. Rev. B: Condens. Matter Mater. Phys.* **2010**, *81*, 195420.
- (44) Papirer, E.; Lacroix, R.; Donnet, J.-B.; Nanse, G.; Fioux, P. XPS Study of the halogenation of carbon black-part 1. Bromination. *Carbon* **1994**, *32*, 1341–1358.
- (45) Widjaja, Y.; Musgrave, C. B. Atomic layer deposition of hafnium oxide: A detailed reaction mechanism from first principles. *J. Chem. Phys.* **2002**, *117*, 1931.
- (46) Hong, S. K.; Song, S. M.; Sul, O.; Cho, B. J. Carboxylic group as the origin of electrical performance degradation during the transfer process of CVD growth graphene. *J. Electrochem. Soc.* **2012**, *159*, K107–K109.
- (47) Leenaerts, O.; Partoens, B.; Peeters, F. M. Adsorption of H<sub>2</sub>O, NH<sub>3</sub>, CO, NO<sub>2</sub>, and NO on graphene: A first-principles study. *Phys. Rev. B: Condens. Matter Mater. Phys.* **2008**, *77*, 125416.
- (48) Liu, L.; Ryu, S.; Tomasik, M. R.; Stolyarova, E.; Jung, N.; Hybertsen, M. S.; Steigerwald, M. L.; Brus, L. E.; Flynn, G. W. Graphene oxidation: thickness-dependent etching and strong chemical doping. *Nano Lett.* **2008**, *8*, 1965–1970.
- (49) Dimiev, A.; Kosynkin, D. V.; Sinitskii, A.; Slesarev, A.; Sun, Z.; Tour, J. M. Layer-by-layer removal of graphene for device patterning. *Science* **2011**, *331*, 1168.
- (50) Datsyuk, V.; Kalyva, M.; Papagelis, K.; Parthenios, J.; Tasis, D.; Siokou, A.; Kallitsis, I.; Galiotis, C. Chemical oxidation of multiwalled carbon nanotubes. *Carbon* **2008**, *46*, 833–840.
- (51) Sreenivasan, R.; McIntyre, P. C.; Kim, H.; Saraswat, K. C. Effect of impurities on the fixed charge of nanoscale HfO<sub>2</sub> films grown by atomic layer deposition. *Appl. Phys. Lett.* **2006**, *89*, 112903.
- (52) Bayerl, A.; Lanza, M.; Aguilera, L.; Port, M.; Nafria, M.; Aymerich, X.; Gendt, S. de Nanoscale and device level electrical behavior of annealed ALD Hf-based gate oxide stacks grown with different precursors. *Microelectron. Reliab.* **2013**, *53*, 867–871.
- (53) Cañado, L. G.; Jorio, A.; Martins Ferreira, E. H.; Stavale, F.; Achete, C. A.; Capaz, R. B.; Moutinho, M. V. O.; Lombardo, A.; Kulmala, T. S.; Ferrari, A. C. Quantifying defects in graphene via Raman spectroscopy at different excitation energies. *Nano Lett.* **2011**, *11*, 3190–3196.
- (54) Zhong, J.-H.; Zhang, J.; Jin, X.; Liu, J.-Y.; Li, Q.; Li, M.-H.; Cai, W.; Wu, D.-Y.; Zhan, D.; Ren, B. Quantitative correlation between defect density and heterogeneous electron transfer rate of single layer graphene. *J. Am. Chem. Soc.* **2014**, *136*, 16609–16617.
- (55) Alles, H.; Aarik, J.; Aidla, A.; Fay, A.; Kozlova, J.; Niilisk, A.; Pärs, M.; Rähn, M.; Wiesne, M.; Hakonen, P.; Sammelselg, V. Atomic layer deposition of HfO<sub>2</sub> on graphene from HfCl<sub>4</sub> and H<sub>2</sub>O. *Central European Journal of Physics* **2011**, *9*, 319–324.
- (56) Jandhyala, S.; Mordí, G.; Lee, B.; Lee, G.; Floresca, C.; Cha, P.-R.; Ahn, J.; Wallace, R. M.; Chabal, Y. J.; Kim, M. J.; Colombo, L.; Cho, K.; Kim, J. Atomic layer deposition of dielectrics on graphene using reversibly physisorbed ozone. *ACS Nano* **2012**, *6*, 2722–2730.
- (57) Martin, M.-B.; Dlubak, B.; Weatherup, R. S.; Yang, H.; Deranlot, C.; Bouzehouane, K.; Petroff, F.; Anane, A.; Hofmann, S.; Robertson, J.; Fert, A.; Seneor, P. Sub-nanometer atomic layer deposition for

spintronics in magnetic tunnel junctions based on graphene spin-filtering membranes. *ACS Nano* **2014**, *8*, 7890.

(58) Geidel, M.; Junige, M.; Albert, M.; Bartha, J. W. In-situ analysis on the initial growth of ultra-thin ruthenium films with atomic layer deposition. *Microelectron. Eng.* **2013**, *107*, 151–155.

(59) Zhao, Y.-P.; Wang, G.-C.; Lu, T.-M.; Palasantzas, G.; Hosson, J.; Th, M. D. Surface/interface-roughness-induced demagnetizing effect in thin magnetic films. *Phys. Rev. B* **1999**, *60*, 1216–1226.

(60) Lin, H. C.; Ye, P. D.; Wilk, G. D. Leakage current and breakdown electric-field studies on ultrathin atomic-layer-deposited Al<sub>2</sub>O<sub>3</sub> on GaAs. *Appl. Phys. Lett.* **2005**, *87*, 182904.

(61) Lee, J. C.; Chen, I. C.; Hu, C. Modeling and characterization of gate oxide reliability. *IEEE Trans. Electron Devices* **1988**, *35*, 2268.